

Journal of Biomedical Optics

BiomedicalOptics.SPIEDigitalLibrary.org

Depth-enhanced fluorescence imaging using masked detection of structured illumination

Joseph Angelo
Vivek Venugopal
Frederic Fantoni
Vincent Poher
Irving J. Bigio
Lionel Herve
Jean-Marc Dinten
Sylvain Gioux

Depth-enhanced fluorescence imaging using masked detection of structured illumination

Joseph Angelo,^{a,b} Vivek Venugopal,^a Frederic Fantoni,^c Vincent Poher,^c Irving J. Bigio,^{b,d} Lionel Herve,^c Jean-Marc Dinten,^c and Sylvain Gioux^{a,*}

^aBeth Israel Deaconess Medical Center, Department of Medicine, 330 Brookline Avenue, Boston, Massachusetts 02215, United States

^bBoston University, Department of Biomedical Engineering, Boston, Massachusetts 02215, United States

^cCEA-LETI, Minatec Campus, Grenoble 38054, France

^dBoston University, Department of Electrical & Computer Engineering, Boston, Massachusetts 02215, United States

Abstract. There is a growing interest in imaging fluorescence contrast at depth within living tissues over wide fields of view and in real time. Most methods used to date to improve depth detection of fluorescence information involve acquisition of multiple images, postprocessing of the data using a light propagation model, and are capable of providing either depth-sectioned or tomographic fluorescence information. We introduce a method, termed masked detection of structured illumination, that allows the enhancement of fluorescence imaging at depth without postprocessing. This method relies on the scanning of a collimated beam onto a turbid medium and the physical masking of the point spread function on the detection arm before acquisition on a CCD camera. By preferentially collecting diffuse photons at a chosen source-detector range, this method enhances fluorescence information at depth and has the potential to form images without postprocessing and in real time. © 2014 Society of Photo-Optical Instrumentation Engineers (SPIE) [DOI: 10.1117/1.JBO.19.11.116008]

Keywords: fluorescence imaging; depth-enhanced imaging; diffuse optical imaging.

Paper 140579PR received Sep. 9, 2014; accepted for publication Oct. 16, 2014; published online Nov. 14, 2014.

1 Introduction

Continuous wave reflectance imaging of exogenous fluorescence in turbid media is relatively superficial, with a maximum detection depth of 5 to 10 mm in the near-infrared (NIR), depending on the medium optical properties.¹ This limitation, in turn, strongly impairs the use of fluorescence imaging during *in vivo* applications in animals or in humans. For example, during the detection of sentinel lymph nodes in breast cancer,² fluorescence imaging performs as well as the detection of ⁹⁹Tcchnetium-colloid except in high body mass index patients, where the presence of fatty tissue strongly limits the depth of detection to <2 to 3 mm.³ Therefore, there is a strong interest in increasing the capabilities of fluorescence imaging to measure signals at depth. Two general approaches are taken to increase the sensitivity to fluorescence at depth. The first approach consists of using ultrasensitive detection technology, such as image intensifiers, intensified CCD, or electron multiplying CCD.⁴⁻⁶ The second approach relies on developing acquisition methods to enhance the sensitivity of fluorescence signals at depth. In this study, we chose the latter approach, since the price of the equipment can be a concern when using highly sensitive detection methods.

Several methods have been developed to perform depth-sensitive measurements within turbid media, each with its own fundamental limitations and benefits. Time- and frequency-domain reflectance methods require the acquisition of several sequential images, or raster scans, to collect a final depth-sensitive map.⁷ This prolonged acquisition usually permits tomographic reconstruction at the cost of lengthy model-based processing. In the spatial domain, laminar optical tomography,⁸⁻¹⁰ while mainly exploited for tomographic reconstructions, could be employed

to perform depth-sensitive fluorescence imaging. However, the acquisition requires two-dimensional raster scanning, the field of view is relatively small, and postacquisition image reconstruction is required. In the spatial-frequency domain, spatial frequency domain imaging has been used for depth-sensitive and tomographic applications over wide fields of view.¹¹⁻¹³ Still, an acquisition requires several images and postprocessing to obtain depth-sensitive images.

In this study, we introduce a novel acquisition method called masked detection of structured illumination (MDSI) that is capable of preferentially enhancing the relative fluorescence signal at depth within a diffuse medium. This spatial-domain method relies on the scanning of a collimated beam onto a diffuse medium and the physical masking of the point spread function (PSF) on the detection arm before acquisition on a CCD camera. By using instrumentation to preferentially collect diffuse photons at a chosen source-detector range, this method shows promise for enhancing fluorescence at depth within the medium. In the first section of this article, we describe the principle of the method and its implementation. In the following section, we present experiments to validate the approach using both digital and physical masks, by imaging fluorescence from various depths inside a tissue-mimicking phantom. Finally, we assess the performance of the method and its current implementation in highlighting deeper or more superficial fluorescence contrast.

2 Materials and Methods

2.1 MDSI Principle

The radial dependence of the backreflectance from a point source illumination in a diffuse medium has been widely

*Address all correspondence to: Sylvain Gioux, E-mail: sgiox@bidmc.harvard.edu

described.¹⁴ From a reflectance imaging perspective, the function that describes this radial dependence can also be called a PSF. This PSF is directly related to the photons' visitation histories between a source and a detector, i.e., the paths most traveled by the collected photons within the medium, often described as a banana-shape function or photon banana. Typically, as the source-detector separation increases, the mean depth of this visitation distribution also increases.¹⁵ As the length of travel increases, photons are more scattered and absorbed by the medium and the PSF intensity decreases. Many studies have taken advantage of this phenomenon to measure information at depth in a diffuse medium^{16,17} or to characterize optical properties.¹⁸ MDSI relies on this principle to preferentially select or reject photons by masking the PSF from a collimated illumination.^{19,20}

As shown in Fig. 1, a laser source is collimated, reflected by a dichroic mirror, and directed onto a diffuse medium (shown in gray). Fluorescence images are formed on a camera through the dichroic mirror and rejecting the excitation light with an emission filter. If two fluorescent inclusions (in green) are present within the medium at different depths and the detection system is scanned across the medium, shorter source-detector separations will excite fluorophores at shallower depth, while longer source-detector separations will excite fluorophores at deeper depths. Therefore, by using a physical mask to block a range of short source-detector separations on the detection path of the system, contributions of deeper fluorophores will be relatively highlighted. Similarly, a different mask can be used to block the longer source-detector separation and highlight the contribution from shallower fluorophores (not shown in Fig. 1).

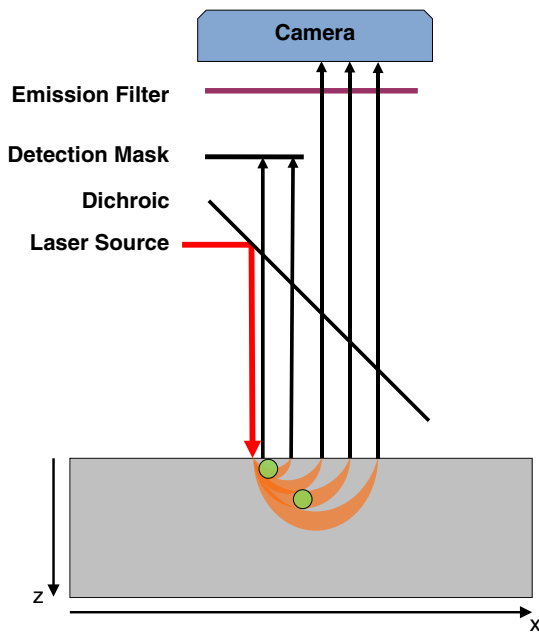


Fig. 1 Masked detection of structured illumination (MDSI)—principle. A point illumination is shined onto a diffuse medium containing two fluorescence inclusions at different depths. Fluorescence is collected through the dichroic mirror and an emission filter in front of a camera. In this geometry, the shallow fluorescent inclusion is optimally excited at shorter source-detection separations and the deeper inclusion at larger source-detection separations. MDSI introduces a mask that preferentially selects the most diffused photons and, therefore, the deeper inclusion in the diffuse medium.

MDSI relies on this core principle to preferentially enhance deeper or shallower contributions to the fluorescence signal. To interrogate the entire medium, and, therefore, form a depth-enhanced fluorescence image, the laser illumination is scanned at regular intervals across the surface of the medium while keeping the mask always centered on the illumination, and images are collected by the camera. One image is acquired per scan location, and all acquired images are summed at the end of the scan to form a final, depth-enhanced fluorescence image.

In this study, we present a possible embodiment for a setup capable of performing the described MDSI and report test results of its performance on the bench.

2.2 System Design

An experimental challenge in building a setup capable of performing MDSI is to guarantee that the physical mask is always centered on the illumination location in the detection path, regardless of the scan position. To achieve this, we built the setup shown schematically in Fig. 2. The source is collimated and then directed onto the sample using a mirror (M_s) that scans the beam over the medium. A first two-lens relay system (L_1 , L_2) is used to relay the image plane from the sample surface to the mask location through the scanning mirror. This guarantees that the illumination is always centered on the physical mask. A second two-lens relay system (L_3 , L_4) is used to relay the masked image back onto the sensor of a CCD camera and descan it to the correct location through a rotating mirror (M_d) that is synchronized with the first scanning mirror. In summary, as the first scanning mirror samples the surface of the medium, the center of the illumination is always at the center of the mask plane, and the resulting masked image is directed to its correct location using the second rotating mirror. In this

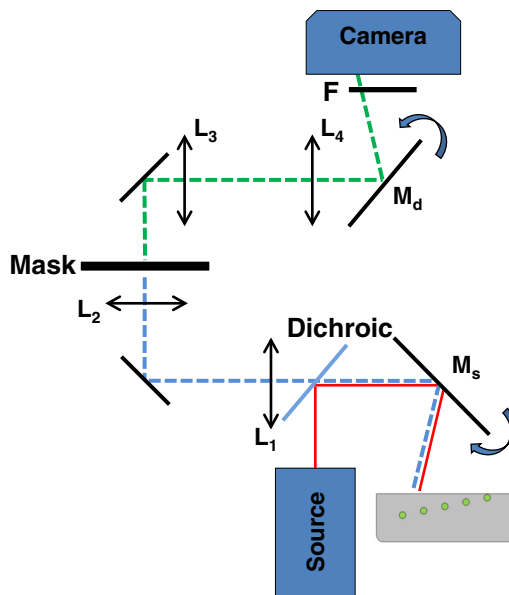


Fig. 2 MDSI—schematics. A source shines a collimated line illumination on the medium via a dichroic mirror and a scanning mirror (M_s). This mirror scans the line illumination over the medium and an image of the fluorescence is formed at the mask plane using a two-lens relay (L_1 and L_2). Note that through this geometry, the illumination is always centered onto the mask plane. An image of the mask plane is formed onto the CCD camera sensor using a two-lens relay (L_3 and L_4) and a descaning mirror (M_d) that replaces the masked image at the correct location onto the CCD sensor.

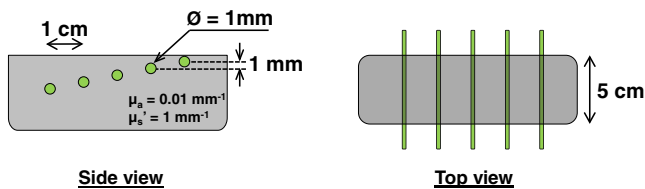


Fig. 3 Schematics of the phantoms used during the experiments. Five capillary tubes are embedded at different depths into a silicon-based tissue-mimicking phantom. Each tube is separated by 1 cm laterally and 1 mm in depth, and is filled with FHI-7206 in dimethyl sulfoxide at a concentration of 3 μ M.

proof-of-concept implementation, the source was shaped as a line, and the scanning was performed along one dimension only.

2.3 Data Acquisition and Processing

In this study, the sample used was a tissue-mimicking, silicone-based phantom having fluorescent tubes at different depths and optical properties of $\mu_s' = 1 \text{ mm}^{-1}$ and $\mu_a = 0.01 \text{ mm}^{-1}$. Titanium dioxide was used as a scattering agent and India ink as an absorbing agent.^{21,22} As shown in Fig. 3, a total of five capillary tubes were embedded within the sample, separated progressively by 1 mm in depth at 1 cm intervals, tube 1 being most superficial and tube 5 being the deepest. Each tube was ~ 1 mm in diameter. The capillary tubes were filled with FHI-7206 (Fabricolor Holding, Paterson, New Jersey) in dimethyl sulfoxide at a concentration of 3 μ M. This dye's maximum absorption is at 720 nm and the emission is strongest at 750 nm, though it continues out to 850 nm. FHI-7206 was chosen because it proved more stable in preliminary testing than other common dyes. Tube depths were sampled individually with the same procedure.

The illumination line was scanned over the sample with 0.25 mm steps. First, a calibration run was performed to synchronize the two rotating mirrors. Following the calibration run, a rapid scan was performed on a homogenous sample to calibrate the camera exposure to collect enough signal at all scan locations (>3000 counts on a 12-bit camera). Finally, the sample was scanned and each image normalized by its optimized exposure before summation. Two types of acquisitions were performed, either with no physical mask (no-mask acquisition) or with a physical mask (mask acquisition) in the detection path of the system. Two types of masks were tested, either center passing or center blocking.

2.4 Simulation Experiments

The concept of MDSI was first tested by simulating the effect of masks onto a no-mask acquisition. Digital masks were created by extrapolating real physical mask profiles to the desired shape or size. Digital masks of blocking width from 0 to 7 mm were used for the center-blocking design, and from 2 to 12 mm passing width for the center-passing design. Following a no-mask acquisition, exposure-normalized images were masked using a digital mask and then summed together.

2.5 Validation Experiments

To validate MDSI, masked images were formed using mask acquisitions (i.e., with a physical mask) and summing the individual exposure-normalized images together. Real masks of 6 mm blocking width (for the center-blocking design) and

3 mm open width (for the center-passing design) were fabricated and tested.

3 Results

3.1 MDSI System

Figure 4 shows an actual photograph of the experimental setup. For the source, a 660 nm 1-W 9-mm laser diode (LDX-3115-660, LDX Optronics, Maryville, Tennessee) was mounted in a temperature-controlled laser diode mount (TCLDM9, Thorlabs, Newton, New Jersey). The laser diode temperature was controlled using a thermoelectric cooler controller (TED200C, Thorlabs) and the intensity using a diode current controller (LDC220C, Thorlabs). The line illumination was formed using a combination of a 50 mm focal length biconvex lens, a 500 mm focal length biconvex lens, and a cylindrical lens having a 3.8 mm focal length. The dichroic mirror used was a 2 in. \times 2 in. 770 nm long-pass interference filter (Chroma, Bellows Falls, Vermont). The scanning was accomplished using standard 2 in. \times 2 in. silver mirrors mounted on stepper motors (HT11-012, Applied Motion, Watsonville, California) and controlled with stepper motor controllers (1240i, Applied Motion). The first two-lens relay system was built using a 50-mm-diameter lens having a 300 mm focal length (L_1) and a 50-mm-diameter lens having a 75 mm focal length (L_2). The second two-lens relay system comprised a 50-mm-diameter lens having a 100 mm focal length (L_3) and a 50-mm-diameter lens having a 75 mm focal length (L_4). Center-blocking masks were made from aluminum shims, while center-passing masks were based on a mechanically variable slit (VA100/M, Thorlabs). Finally, the camera used was a monochrome 12-bit cooled CCD (Hamamatsu Orca-ER, Bridgewater, New Jersey) and the emission filter a 25-mm-diameter 795 nm long-pass interference filter (HHQ795LP, Chroma).

Shown in Fig. 5 are sample images and corresponding line profiles taken during a mask acquisition (center-blocking design) of a single tube, as well as the resulting summed image using the MDSI system. As anticipated, both the images and line profiles clearly show the overlapping illumination and real mask scanning over the tube containing the fluorophore.

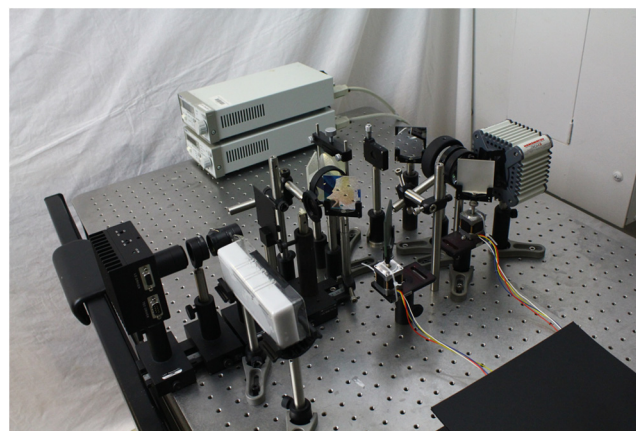


Fig. 4 Photograph of the MDSI setup. As shown in the schematics in Fig. 2, a source shines a collimated beam through a dichroic mirror and a scanning mirror. An image of the phantom is formed at the mask plan and a secondary image for the masked phantoms reformed on the CCD sensor.

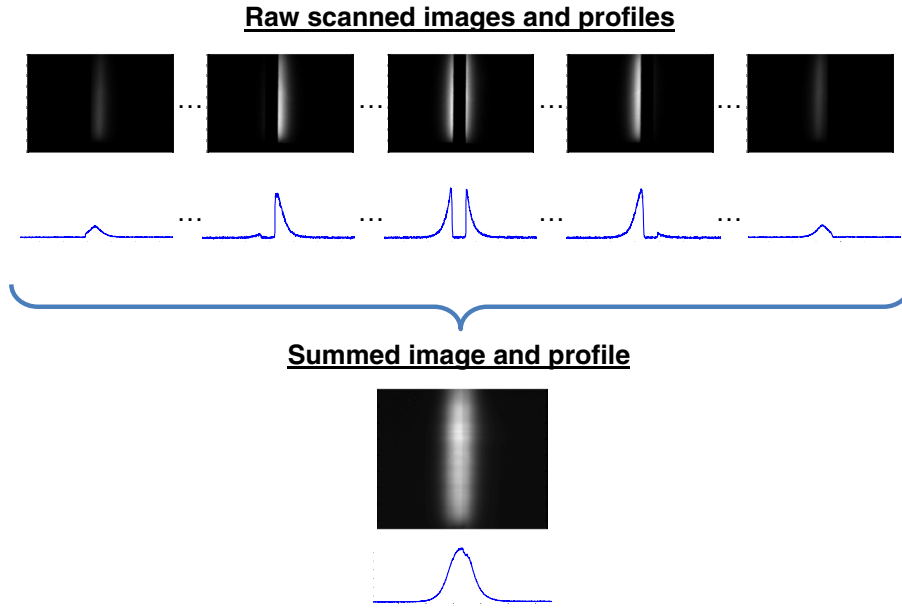


Fig. 5 Sample images and corresponding profiles obtained with the MDSI setup. As the illumination scans the medium, the mask (center blocking) is centered on the illumination and blocks the less diffused photons. The summed image is formed by individually summing all masked images.

3.2 Center-Blocking Simulation Experiments

In this experiment, several digital center-blocking masks of varying size, from 0 to 7 mm blocking width, were applied to no-mask acquisitions. As illustrated in Fig. 6(a), for a fixed 6-mm real mask size, the fluorescence from shallower tubes is relatively more attenuated compared to deeper tubes, showing a relative enhancement of fluorescence signal at depth. To

quantify this effect, the ratios of the peak for a given digital center-blocking mask scan to that of the no-mask case were simulated at various mask sizes without averaging, and are shown in Fig. 6(b). Going from a 0-mm mask (i.e., no-mask) to a 7-mm mask, the peak signal for tube 1 decreases by 76%. Similarly, peaks for tubes 2, 3, 4, and 5 exhibit decreases by 70, 64, 60, and 54%, respectively, demonstrating less attenuation for

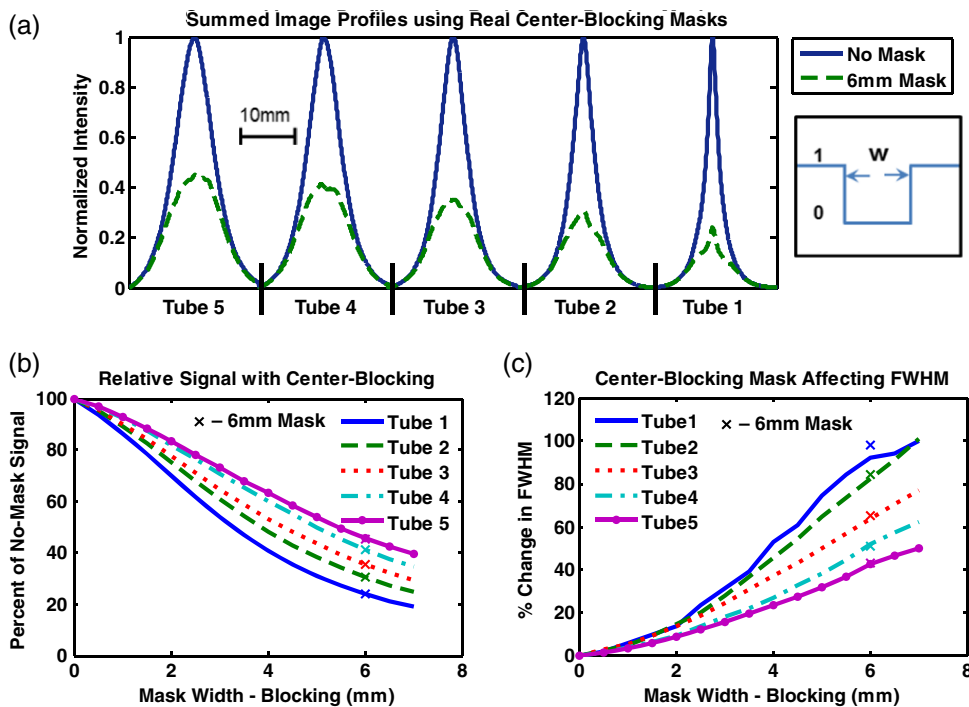


Fig. 6 Center-blocking mask results. (a) compares the summed images profiles for the no-mask scan and the real 6 mm mask scan. Note the relative signal and full-width at half-maximum (FWHM) increase for deeper tubes when the center-blocking mask is used. Digital mask simulations (lines) demonstrate this effect showing (b) the relative signal increase and (c) the FWHM with increasing blocking width and tube depth, along with the real 6 mm mask scans (x's).

deeper signals. In addition, a broadening of the profiles [demonstrated in Fig. 6(a)] is noticeable as the mask size increases, which is consistent with the fact that a greater proportion of diffused photons is collected. This broadening is characterized by the full-width at half-maximum (FWHM) of the emission line profiles for digital masks and is shown in Fig. 6(c). The percent increase in FWHM from a no-mask scan to a 7-mm center-blocking scan is 100, 100, 77, 62, and 50% for tubes 1, 2, 3, 4, and 5, respectively. In addition, results obtained with the 6-mm center-blocking real mask are plotted in Figs. 6(b) and 6(c) (x's) for comparison with the digital mask data.

3.3 Center-Passing Simulation Experiments

In this experiment, several digital center-passing masks of varying sizes from 12 to 2 mm width were applied to no-mask acquisitions. As shown in Fig. 7(a), for a fixed 3-mm real mask size, the fluorescence from deeper tubes is relatively more attenuated compared to shallower tubes, showing a relative enhancement of the fluorescence signal at the surface. To quantify this effect, the ratios of the peak for a given digital center-passing mask scan to that of the no-mask case were simulated at various mask sizes, without averaging, and are shown in Fig. 7(b). Comparing results from the no-mask [Fig. 7(b), asterisk] to a 2-mm mask, the peak signal for tube 1 decreases by 63%. Similarly, peaks for tubes 2, 3, 4, and 5 exhibit decreases of 69, 71, and 77%, respectively, demonstrating more attenuation for deeper signals. In addition, a narrowing of the image profiles is noticeable as the mask size decreases, which is consistent with the fact that a greater proportion of diffused photons is rejected. This narrowing is characterized by the FWHM and is shown in Fig. 7(c). The decrease in FWHM is 19, 25, 33, 21, and 28% drop for tubes 1, 2, 3, 4, and 5, respectively. In addition, the

no-mask condition (asterisks) and the 3 mm center-passing physical mask (x's) results are plotted in Figs. 7(b) and 7(c) for comparison with the digital mask data.

3.4 Validation Experiments

A set of summed images obtained with no mask, a real 6 mm center-blocking mask, and a real 3 mm center-passing mask is shown for all tubes in Fig. 8. Each row of images is normalized to tube 1 of the row. Line profiles for center-blocking and center-passing masks are normalized by and compared to the no-mask case in Figs. 6(a) and 7(a), respectively. Again, it is evident that the relative effect on deeper, more diffused signals is less for center-blocking scans and more for center-passing scans. As evidenced in the previous experiments (Secs. 3.3 and 3.4), compared to a no-mask acquisition, the center-blocking mask shows more diffuse images with higher levels of fluorescence at deeper locations. The center passing, conversely, shows less diffuse images with lower fluorescence levels.

Results obtained with these validation experiments were compared to simulations performed previously and indicated in plots in Figs. 6(b), 6(c), 7(b), and 7(c). Overall, they show good agreement with the simulation data.

4 Discussion

In this study, we introduce and validate a novel acquisition method, called MDSI, taking advantage of the diffusion of photons within a turbid medium to preferentially enhance fluorescence signal as a function of depth in an imaging geometry. In this particular embodiment, the method enables performance of depth-enhanced fluorescence imaging without any

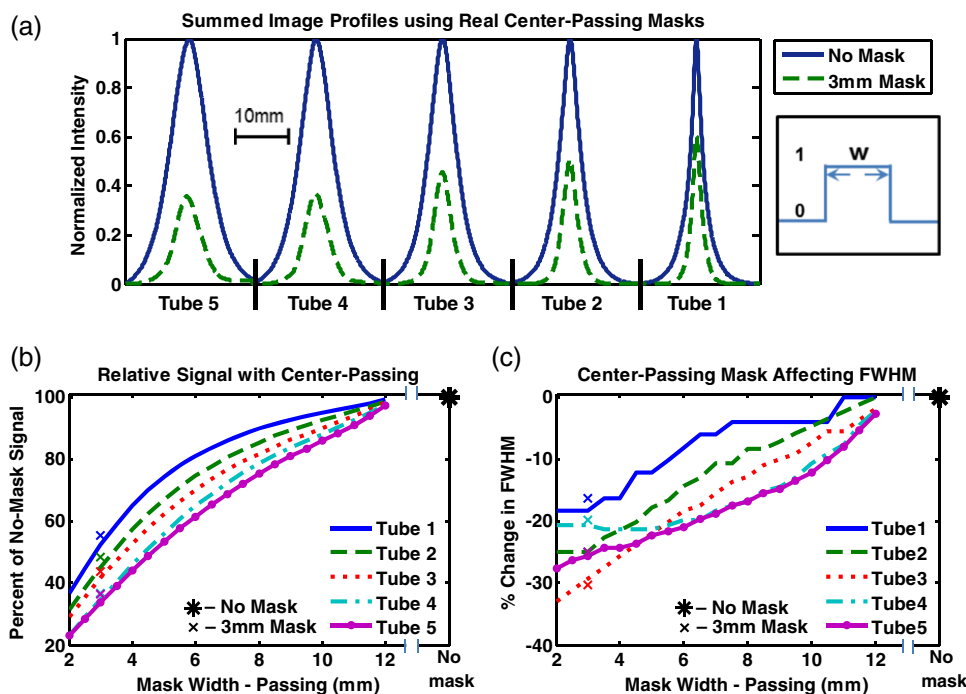


Fig. 7 Center-passing mask results. (a) compares the summed images profiles for the no-mask scan and the real 3 mm mask scan. Note the relative signal and FWHM decrease for deeper tubes when the center-passing mask is used. Digital mask simulations (lines) demonstrate this effect by showing (b) the relative signal decrease and (c) the FWHM with decreasing passing width and tube depth, along with the real 3 mm mask (x's) and no-mask (asterisks) scans.

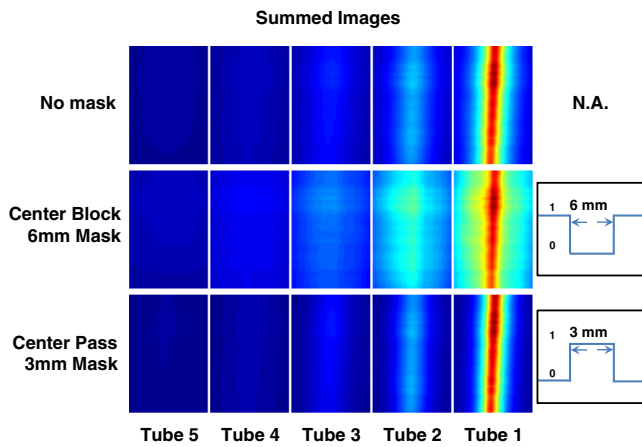


Fig. 8 Images for all tubes formed by physically masked scans. The blurring and signal enhancement is apparent between the no-mask case and the center block 6 mm mask case. Likewise, sharpening and signal decrease is apparent for the center pass 3 mm mask case.

postprocessing, simply relying on an optical arrangement to either mask or select diffuse photons in a scanning geometry.

We investigated the effect of different mask sizes and shapes. Because the selection of the mask is of paramount importance with MDSI, a large body of work remains to be completed by studying different mask shapes and understanding their effects. In addition, the current implementation is focused on fluorescence imaging, but because MDSI highlights diffusion effects, it is anticipated that this method could also be used without fluorescence to highlight changes in absorption and/or scattering without postprocessing.

The phantom used in this study consists of tissue-simulating material without autofluorescence since the motivation for this study was to prove the potential of MDSI for signal depth enhancement. In our case, in the NIR range around 800 nm, tissue autofluorescence in living tissues is particularly low²³ and should not present any concern. However, if this technique is applied to lower wavelengths, where autofluorescence becomes significant, such as <700 nm, this method may be prone to collect nonspecific diffused fluorescence, which would lower its performances.

Some of the limits concerning signal depth and mask size were reached in this study. Though the percent change in relative signal increases with increasing center-blocking mask width for each tube [see Fig. 6(b)], the absolute signal also decreases [Figs. 6(a) and 8]. Tube 1's signal decreases faster than deeper tubes' signals, but exposure time and signal noise become a concern when using wide masks with deeper tubes. For the center-passing mask case, mask widths narrower than 3 mm tend to create sampling artifacts, causing the relative signal to fluctuate and seem nonmonotonic. These sampling artifacts can be avoided by using a higher spatial sampling. Finally, the center-pass effect of narrowing a signal's FWHM for the deepest tubes (4 and 5) begins to diminish at ~5 mm masks or smaller. This is thought to be due to the absolute signal of these deeper tubes reaching the noise floor. All measurements were made on a homogenous phantom, and the performance of this method on heterogeneous media will be the topic of future investigation.

One of the limitations of the current setup is a long acquisition time due to a calibration run followed by data acquisition, all in a step-by-step scanning manner. More particularly, the current setup has the disadvantage of keeping the collimated laser

line at the same position for a long time. This causes the fluorescence signal to bleach over time and is the reason behind the choice of laser dye, which is more stable in these conditions. However, the current setup acquisition is not optimized, scanning could be performed more rapidly, and the source could be synchronized with the image acquisition. Also, the development of a continuously scanning instrument would eliminate this effect.

A strong motivation for developing MDSI is the potential to provide rapid (near to real time) depth-enhanced fluorescence imaging. As detailed above, the current system relies on a step-by-step scanning approach, requiring postacquisition summation of the images and rendering the acquisition slow. Because MDSI relies only on masked scanning of the medium without postprocessing, it is possible to add a continuously rotating polygonal mirror along with continuous acquisition on a CCD camera for real-time summation of masked images and, therefore, real-time depth-enhanced fluorescence imaging.

The similarity of MDSI to other diffuse optics techniques has been described above. Some similarities can be seen between MDSI and microscopy techniques such as confocal microscopy, but the techniques function according to different principles. MDSI relies on highly scattering media in order for the structured illumination to propagate diffusely and to sample select depths on average according to the source-detector separation. Sufficient scattering is necessary for MDSI to work, whereas most microscopy techniques suffer greatly from noise due to light scattering within the sample.

5 Conclusion

In this study, we introduce and validate an acquisition method, called MDSI, allowing performance of depth-enhanced fluorescence imaging from a diffusive medium without postprocessing. We present a proof-of-concept instrument and perform simulation experiments using digital masks to investigate the effect of mask size and shape, as well as validate MDSI capabilities with a physical blocking and passing masks. In summary, this study lays the foundation for the development of a rapid *in vivo* depth-enhanced fluorescence imaging method without postprocessing.

Acknowledgments

The authors would like to thank John V. Frangioni and Caroline Boudoux for many helpful discussions. We would also like to thank David Burrington, Jr. for editing and Eugenia Trabucchi for administrative assistance. This work was supported by NIH/NCATS Award Number 8 UL1 TR000170-05 to Harvard Clinical and translational Science Center, collaboration Award Number 027343.386541.05226, and NIH/NIDDK Award Number K01-DK-093603. Joseph Angelo was supported by a National Science Foundation Graduate Research Fellowship under Award Number DGE-1247312.

References

1. S. Gioux, H. S. Choi, and J. V. Frangioni, "Image-guided surgery using invisible near-infrared light: fundamentals of clinical translation," *Mol. Imaging* **9**(5), 237–255 (2010).
2. S. L. Troyan et al., "The FLARE intraoperative near-infrared fluorescence imaging system: a first-in-human clinical trial in breast cancer sentinel lymph node mapping," *Ann. Surg. Oncol.* **16**(10), 2943–2952 (2009).

3. F. P. Verbeek et al., "Near-infrared fluorescence sentinel lymph node mapping in breast cancer: a multicenter experience," *Breast Cancer Res. Treat.* **143**(2), 333–342 (2014).
4. S. Gioux et al., "Low-frequency wide-field fluorescence lifetime imaging using a high-power near-infrared light-emitting diode light source," *J. Biomed. Opt.* **15**(2), 026005 (2010).
5. B. Zhu et al., "Validating the sensitivity and performance of near-infrared fluorescence imaging and tomography devices using a novel solid phantom and measurement approach," *Technol. Cancer Res. Treat.* **11**(1), 95–104 (2012).
6. K. Sexton et al., "Pulsed-light imaging for fluorescence guided surgery under normal room lighting," *Opt. Lett.* **38**(17), 3249–3252 (2013).
7. B. Pogue et al., "Comparison of imaging geometries for diffuse optical tomography of tissue," *Opt. Express* **4**(8), 270–286 (1999).
8. E. M. C. Hillman et al., "Laminar optical tomography: demonstration of millimeter-scale depth-resolved imaging in turbid media," *Opt. Lett.* **29**(14), 1650–1652 (2004).
9. S. Yuan et al., "Three-dimensional coregistered optical coherence tomography and line-scanning fluorescence laminar optical tomography," *Opt. Lett.* **34**(11), 1615–1617 (2009).
10. L. Zhao et al., "The integration of 3-D cell printing and mesoscopic fluorescence molecular tomography of vascular constructs within thick hydrogel scaffolds," *Biomaterials* **33**(21), 5325–5332 (2012).
11. D. J. Cuccia et al., "Modulated imaging: quantitative analysis and tomography of turbid media in the spatial-frequency domain," *Opt. Lett.* **30**(11), 1354–1356 (2005).
12. S. D. Konecky et al., "Quantitative optical tomography of sub-surface heterogeneities using spatially modulated structured light," *Opt. Express* **17**(17), 14780 (2009).
13. A. Mazhar et al., "Structured illumination enhances resolution and contrast in thick tissue fluorescence imaging," *J. Biomed. Opt.* **15**(1), 010506 (2010).
14. T. J. Farrell, M. S. Patterson, and B. Wilson, "A diffusion theory model of spatially resolved, steady-state diffuse reflectance for the noninvasive determination of tissue optical properties in vivo," *Med. Phys.* **19**(4), 879–888 (1992).
15. W. Cui, N. Wang, and B. Chance, "Study of photon migration depths with time-resolved spectroscopy," *Opt. Lett.* **16**(21), 1632–1634 (1991).
16. T. J. Pfeifer et al., "Selective detection of fluorophore layers in turbid media: the role of fiber-optic probe design," *Opt. Lett.* **28**(2), 120–122 (2003).
17. C. Zhu, Q. Liu, and N. Ramanujam, "Effect of fiber optic probe geometry on depth-resolved fluorescence measurements from epithelial tissues: a Monte Carlo simulation," *J. Biomed. Opt.* **8**(2), 237–247 (2003).
18. R. Doornbos et al., "The determination of in vivo human tissue optical properties and absolute chromophore concentrations using spatially resolved steady-state diffuse reflectance spectroscopy," *Phys. Med. Biol.* **44**(4), 967 (1999).
19. J. Angelo et al., "Masked detection of structured illumination (MDSI): depth sensitive fluorescence measurement," *Proc. SPIE* **8578**, 85780Q (2013).
20. F. Fantoni et al., "Laser line scanning illumination scheme for the enhancement of contrast and resolution for fluorescence reflectance imaging," *Proc. SPIE* **8572**, 85720L (2013).
21. F. Ayers et al., "Fabrication and characterization of silicone-based tissue phantoms with tunable optical properties in the visible and near infrared domain," *Proc. SPIE* **6870**, 687007 (2008).
22. B.W. Pogue and M. S. Patterson, "Review of tissue simulating phantoms for optical spectroscopy, imaging and dosimetry," *J. Biomed. Opt.* **11**(4), 041102 (2006).
23. J. V. Frangioni, "In vivo near-infrared fluorescence imaging," *Curr. Opin. Chem. Biol.* **7**(5), 626–634 (2003).

Biographies of the authors are not available.